International Journal of Emerging Technology in Computer Science & Electronics (IJETCSE)
ISSN: 0976-1353 Volume 14 Issue 1 –APRIL 2015.

DYANAMIC ANALYSIS OF DC-DC CONVERTER INTERNAL TO STAND ALONE PV /BATTERY POWER SYSTEMS

P.PRIYA, Mrs.D.VIMALA, *M.E,*
Department of electrical and electronics engineering
Pgp college of engineering and technology namakkal, tamilnadu

Abstract

A three-port DC–DC converter integrating photovoltaic (PV) and battery power for high step-up applications is proposed in this paper. The topology includes five power switches, two coupled inductors, and two active-clamp circuits. The coupled inductors are used to achieve high step-up voltage gain and to reduce the voltage stress of input side switches. Two sets of active-clamp circuits are used to recycle the energy stored in the leakage inductors and to improve the system efficiency. The operation mode does not need to be changed when a transition between charging and dis-Charging occurs. Moreover, tracking maximum power point of the source and regulating the output voltage can be operated simultaneously during charging/discharging transitions. As long as the sun irradiation level is not too low, the maximum power point tracking (MPPT) algorithm will be disabled only when the battery charging voltage is too high. Therefore, the control scheme of the proposed converter provides maximum utilization of PV power most of the time. As a result, the proposed converter has merits of high boosting level, reduced number of devices, and simple control strategy. Experimental results of a 200-W laboratory prototype are presented to verify the performance of the proposed three-port converter.

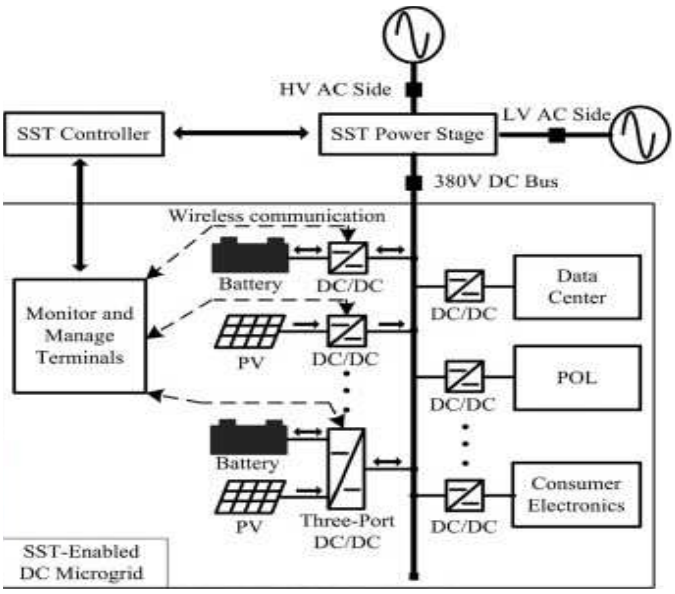

Fig. 1. Part of the FREEDM system diagram showing an SST-enabled DC Micro grid.

I.INTRODUCTION

Integrated multiport converters for interfacing several Power sources and storage devices are widely used in recent years. Instead of using individual power electronic converters for each of the energy sources, multiport converters have the ad-vantages including less components, lower cost, more compact size, and better dynamic performance. In many cases, at least one energy storage device should be incorporated. For example, in the electric vehicle application, the regenerative energy occurs during acceleration or startup. Therefore, it is very important for the port connected to the energy storage to allow Bidirectional power flow. Various kinds of topologies have been proposed due to the advantages of multiport converters. The combination strategies for the multiport converter include sharing switches, capacity-tors, inductors, or magnetic cores [1]. One could select a proper topology by considering many aspects such as cost, reliability, and flexibility depending on the applications. An application of hybrid energy supply using renewable energy sources and storage devices is shown in Fig. 1Centralized control of the proposed converter. Therefore, the system cost and volume can be reduced. The major contribution of this paper is to propose an integrated three-port converter as anon isolated alternative other than typical isolated topologies forhigh step-up

The detailed analysis is given in the following sections: The principle of operation is described in Section II. The PV source modeling, topological modes, and ZVS conditions are analyzed in Section III. The modeling and control strategy is explained in Section IV. Finally, the experimental results are presented in Section V

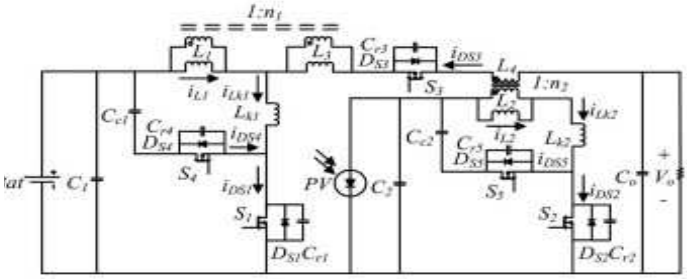

Fig.2-Topology of the proposed converter

II. PRINCIPLE OF OPERATION

This section introduces the topology of proposed non isolated three-port dc–dc converter, as illustrated in Fig. 2. The converters composed of two main switches S_1 and S_2 for the battery and PV port. Synchronous switch S_3 is driven complementarily tos$_1$ such that bidirectional power flow for the battery port canbe achieved. Two coupled inductors with winding ratios n_1 andn_2 are used as voltage gain extension cells. Two sets of active-clamp circuits formed by S_4 ,$L_{k\,1}$, C_{c1} and S_5 , $L_{k\,2}$, C_{c2} are usedto recycle the leakage energy. $L_{k\,1}$ and $L_{k\,2}$ are both composedof a small leakage inductor from the coupled inductor and anexternal leakage inductor. Two independent control variables, duty cycles d_1 and d_2 , allow the control over two ports of theconverter, while the third port is for the power balance.

Thefixed-frequency driving signals of the auxiliary switches S_3 ands_4 are complementary to primary switch S_1 . Again, S_3 providesa bidirectional path for the battery port. Similarly, S_5 is drivenin a complementary manner to S_2 . A 180◦ phase shift is appliedbetween the driving signals of S_1 and S_2 .
There are four operation periods based on the available solar Power. First, the sun is in the eclipse stage and the solar irradiation is either unavailable or very low. This operation periodic defined as period 1, and the battery will serve as the main power source. As the sun starts to shine and the initial solar irradiation is enough for supplying part of the load demand, the operation period is changed to period 2. The load is supplied by both solar and battery power in this period. For period 3, the increasing isolation makes the solar power larger than the load demand. The battery will preserve extra solar power for backup use. During period 4, the charging voltage of the battery reaches the preset level and should be limited to prevent overcharging. According to the solar irradiation and the load demand, the proposed three-port converter can be operated under two modes. In the battery balance mode (mode 1), maximum power point tracking (MPPT) is always operated for the PV port to draw maximum power from the solar panels. The battery port will maintain the power balance by storing the unconsumed solar power during light-load

$$P_{load}= P_{pv\ SVC} + P_{bat} \quad (1)$$

condition or providing the power deficitduring heavy-load condition. The power sharing of the inputscan be represented as

Where P_{load} is the load demand power, $P_{pv\ SVC}$ is the PV power under solar voltage control (SVC), and $P_{bat\ SVC}$ is the battery power under SVC. In mode 1, maximum power is drawn from the PV source. The battery may provide or absorb power depending on the load demand. Therefore, $P_{bat\ SVC}$ could be either positive or negative. When the battery charging voltage is higher than the maximum setting, the converter will be switched into battery management mode (mode 2). In mode 2, MPPT will be disabled; therefore, only part of the solar power is drawn. However, the battery voltage could be controlled to protect the battery from overcharging. The power sharing of the inputs can be represented as

$$P_{load}= P_{pv\ BVC} + P_{bat\ BVC} \quad (2)$$

Where $P_{pv\ BVC}$ is the PV power under battery voltage control (BVC) and $P_{bat\ BVC}$ is the battery charging power under SVC.
If the load is increased and the battery voltage is reduced, the converter will be switched to mode 1. The output voltage is always kept at 380 V in both modes.

III. TOPOLOGICAL MODES AND ANALYSIS

It is well explained in the literature that using aPV generator as input source has significant effect on the converter dynamics. The nonlinear V −I characteristic of a Generator can be modeled using current source, diode, and resistors. The single-diode model shown in Fig. 3(a) is widely used for the PV source modeling. This model provides a trade-off between accuracy and complexity. Theremin's equivalent model with non-constant voltages and resistances has beenproposed to closely approximate the characteristic of PV generator. The Theremininbased model provides simpler prediction and computation for the maximum power point ofPV array under different operating conditions.

Theremin's theorem is not valid for a nonlinear model, but the nonlinear model could be represented by a linear one with non-constantparameters. In for example, the piece-wise linearization is used to linearize the diode. The parameters in Fig. 3(a) can be estimated using the manufacturer's datasheet. As shown in Fig. 3(b), the actual diode characteristic has been divided into three regions and the characteristic

In each region is approximated as a straight line. Each line can be further represented by a set of voltage source $V_{x,n}$and resistance one of the boundary points such that the operation at this pointhas no approximation error. The single-diode model of the PVgenerator with linearized diode is shown in Fig. 3(c), where thediode is approximated by the voltage source V_x, and resistanceR_D . The values of $V_x$and R_D are dependent on the operation region of the PV generator. The Theremin's equivalent model.

Fig. 3(c) is shown in Fig. 3(d). From the derivation in ,the$v_{pvth,n}$and $R_{pvth,n}$can be calculated by

$$V_{pv} = V_{x,n}+ R_{D,n} \cdot \frac{R_{sh} \cdot I_{ph} - V_{x,n}}{R_{sh}+ R_{D,n}} \quad (3)$$

$$Rpv=Ra + \frac{R_{sh} \cdot R_{D,n}}{R_{sh}+ R_{D,n}} \quad (4)$$

For the following discussion, the Theremin's equivalent modelis adopted for the PV generator modeling.

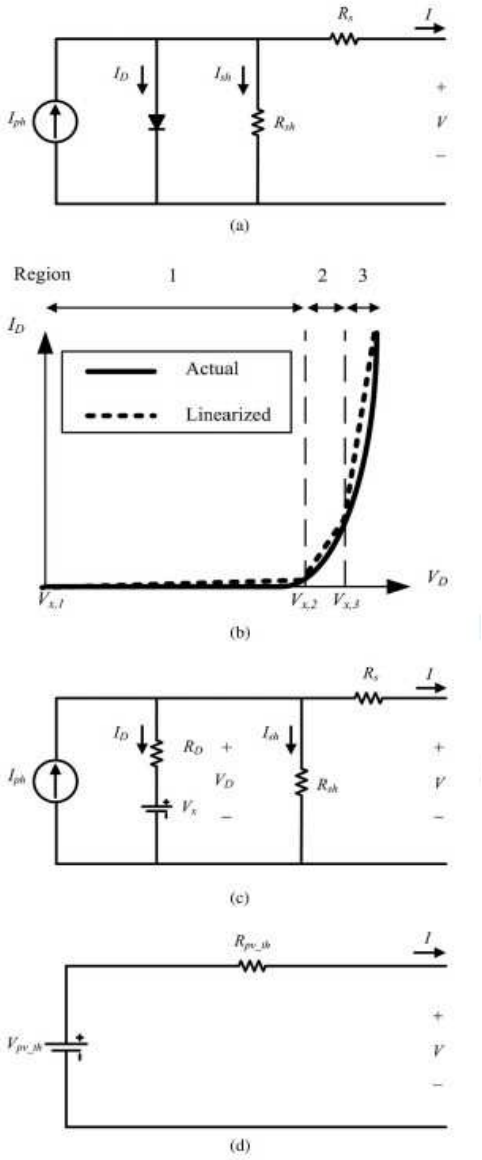

Fig. 3.Theremin's equivalent circuit derived from the single-diode model.
a. Single-diode model of a PV generator
b. V −I characteristic of diode: actual and linear approximation [34].
c. Single-diode model with linearized diode.
d. Theremin's equivalent circuit for a single-diode model with linearized.

$R_{D,n}$(n = 1,2,3). The approximation of piecewise linearization would be more accurate as the number of regions increased. At the boundary points of regions, the values of linearized characteristic are exactly the same as actual characteristic. Therefore, the maximum power point of the PV generator is chosen as

B. Operation Of The Topological Modes

Before performing the analysis, some assumptions should be made: 1) the switches are assumed to be ideal; 2) the magnetizing inductors are large enough so that the current flowingthrough the inductors is constant; 3) the capacitors are large enough so that the voltages across the capacitors are constant. The topological modes over a switching cycle are shown inFig. 4 and key waveforms of the proposed converter are given inFig. 5. Detailed explanation of each interval is given as follows: Interval 1 [see Fig. 4(a), $t_0 \le t < t_1$]: At t_0 , S_1 and auxiliary switches S_4 and S_5 are turned OFF, while primary switch S_2 is turned ON. Although S_1 is in the off state, resonant inductor L_{k1}resonates with C_{r1} and C_{r4} . In this period, C_{r1} is discharged to zero and C_{r4} is charged to $V_{bat}+ V_{Cc1}$. For the PV port,$S_2$is turned ON and the current from the PV panels flowsthrough $V_{pvth}- L_2 - L_{k2} - S_2$ loop. In order to achieve theZVS feature for S_1 , the energy stored in resonant inductor L_{k1}should satisfy the following inequality:

$$L_{k1} \ge (C_{r1} \; C_{r4})[v_{ds1}(t_0)]^2 . [i_{lk1}(t_0)]^2$$

Interval 2 [see Fig. 4(b), $t_1 \le t < t_2$]: This mode starts whenv_{ds1} is down to zero. The body diode of S_1 is forward biasedso that the ZVS condition for S_1 is established. The resonantCurrenti_{lk1} is increased toward zero. L_2 is still linearly charged in this period. Interval 3 [see Fig. 4(c), $t_2 \le t < t_3$]: S_1 begins to con-duct current at t_2 and the battery port current follows the path $_{bat}-L_1-L_{k1}-S_1$. S_2 is also turned ON in this interval. There-fore, both L_1 and L_2 are linearly charged and energy of both input ports is stored in these magnetizing inductors. Auxiliaryswitches S_3 , S_4 , and S_5 are all turned OFF. Interval 4 [see Fig. 4(d), $t_3 \le t < t_4$]: In this interval, S_2 starts to be turned OFF and the auxiliary switch S_5 remains in the OFF state. However, a resonant circuit formed by L_{k2} , C_{r2} , and C_{r5}releases the energy stored in L_{k2} . Resonant capacitor C_{r2} is quickly charged to $V_{pvth}+ V_{Cc2}$, while C_{r5} is discharged to zero. In order to achieve the ZVS feature for S_5 , the energy stored in resonant inductor L_{k2} should satisfy the following that the C_{r5} is much smaller than C_{c2} , almost all the magnetizing currents are recycled to charge the clamp capacitor C_{c2} .Furthermore, V_{Cc2} is considered as a constant value since the capacitance of C_{c2} is large enough. This interval ends wheninductor current i_{lk2} drops to zero.

Interval 6 [see Fig. 4(f), $t_5 \le t < t_6$]: At t_5 , the current ofL_{k2} is reversed in direction and energy stored in t_5 is releasedthrough the $C_{c2}-S_5-L_{k2}-L_3$ loop. This interval ends whenS_5 is turned OFF.

Interval 7 [see Fig. 4(g), $t_6 \le t < t_7$]: Switches S_2 and $s_5$are both in the OFF state at t_6 . A resonant circuit is formed byL_{k2} , C_{r2} , and C_{r5} . During this interval, C_{r2} is discharged to zero and C_{r5} is charged to $V_{pvth}+ V_{Cc2}$. To ensure the ZVSswitching of S_2 , the energy stored in L_{k2} should be greater thanthe energy stored in parasitic capacitors C_{r2} and C_{r5}

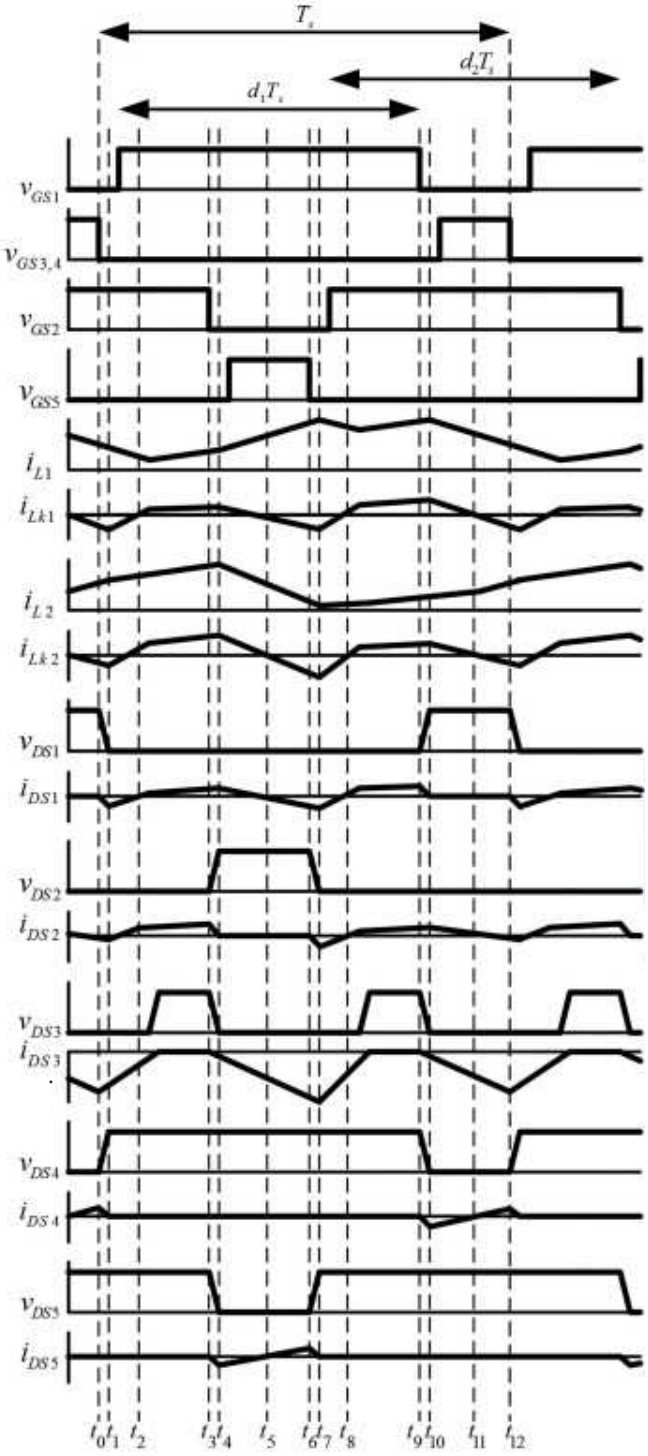

Fig. 5.
Key waveforms of the proposed converter.

$$L_{k2} \geq (C_{r2} + C_{r5})[v_{ds2}(t_6)]^2 \cdot [i_{lk2}(t_6)]^2 \quad (7)$$

Interval 8 [see Fig. 4(h), $t_7 \leq t < t_8$]: This interval starts when the voltage across C_{r2} is zero and the body diode D_{s2} is turnedON. Leakage inductor current i_{lk2} is linearly increased andthe secondary-side current of the coupled inductor is increasedas well. The main switch S_2 should be turned ON before i_{lk2}becomes positive to ensure ZVS operation. Interval 9 [see Fig. 4(i), $t_8 \leq t < t_9$]: The circuit operationof interval 9 is identical to interval 3 since S_1 and S_2 are turnedON in both intervals. Interval 10 [Fig. 4(j), $t_9 \leq t < t_{10}$]: At t_9 , S_1 is turned OFF,while S_3 and S_4 remain in OFF state. During this interval, L_{k1}will resonant with C_{r1} and C_{r4} to release the energy trappedin it. Resonant capacitor

$$L_{k1} \geq (C_{r1} + C_{r4})[v_{ds4}(t_9)]^2 \cdot [i_{lk1}(t_9)]^2 \quad (8)$$

C_{r1} is charged to $V_{bat} + V_{Cc1}$, whileC_{r4} is discharged to zero. To achieve the ZVS feature for S_4 ,the energy stored in resonant inductor L_{k2} should satisfy thefollowing inequality:

Interval 11 [see Fig. 4(k), $t_{10} \leq t < t_{11}$]: This interval beginswhen v_{ds4} drops to zero and the body diode across S_4 is turnedON. The ZVS condition for S_4 is then established. Almost allthe magnetizing current is recycled to charge C_{c1} since $C_{r4}$is much smaller than C_{c1} . Moreover, V_{Cc1} is considered as aconstant value since the capacitance of C_{c1} is large enough. Thisinterval ends when inductor current i_{lk1} reaches zero. Interval 12 [see Fig. 4(l), $t_{11} \leq t < t_{12}$]: The current flowthrough L_{k1} is reversed in direction at t_{11} , and the energy storedin C_{c1} is released through the $C_{c1} - S_4 - L_{k1} - L_1$ loop. Thisinterval ends when S_4 is turned OFF and the operation of theproposed converter over a switching cycle is complete.

(6) C. ZVS Analysis:

According to the (5)–(8), ZVS at turn-on transition could beachieved when enough energy is stored in the leakage inductorsL_{k1} and L_{k2} . The ZVS conditions for switches $S_1 - S_4$ shouldbe determined by (5) and (7) since the ZVS transient periods ofswitches S_1 and S_2 can be expressed as

$$V_{ds1} = V_{bat} + V_{Cc1} = \frac{V_{bat}}{1 - d_1} \quad (9)$$

$$V_{ds2} = V_{pv} \cdot \frac{V_{pvth}}{1 - d_2} \quad (10)$$

Where η represents the converter efficiency. It is noted that as L_{k1} and $L_2L_{k\ 2}$, the behavior of the con-long as L_1Verter duty cycle is approximately the same as for the non-active-Clamp converter in the continuous conduction mode. Typically,$L_{k\ 1} = L_1$ /10 and $L_{k\ 2} = L_2$ /10 can be the conservative designGuidelines. The effective duty cycles d_{eff1} and d_{eff2} are assumedTobe equal to d_1 and d_2 for subsequent equations. As a result, the following inequalities can be derived from (9)–(12) toDetermine a proper leakage inductor.

IV. MODELING AND CONTROL STRATEGY

As mentioned in Section II, the operation modes of the converter are determined by the conditions of available solar power Andbattery charging states. Controlling the converter in eachMode requires different state variables to regulate voltages ofThe input and output ports. There are three control loops for theProposed converter: output voltage control (OVC), SVC, and BVC. The control scheme is shown in Fig. 6. The OVC is aSimple voltage regulation loop.

The SVC and BVC loops shareThesame control variable d_2 to achieve smooth mode transitions. SVC is used to regulate the voltage of the PV port and Implementthe MPPT algorithm. BVC is the battery voltage regulationloop to prevent overcharging. It is noted that the PV Portisoperated under SVC most of the time. Therefore, BVC would Notbe active under normal operation. Only one control loop be-Tween SVC and BVC is performed.

Moreover, once BVC startsTo take control over d_2 , SVC will be disabled immediately toAvoid the noise issue caused by the MPPT algorithm . InFact, the cross-coupled control loops is the intrinsic feature ofThemultiport converters since it is a high-order system. It willBea challenge to design the controllers of a multiport converter.The decoupling network for extracting separate transfer functionsin such a system has been introduced by describing theSystem dynamics in a matrix.

The small-signal modeling method is widely used for thePower electronics converter. For a three-port converter that hastwoinput ports, a matrix-form model will be very helpful to Implement the closed-loop control and analyze the system dynamics. Since there are two operation modes for the proposed Three-port converter, two sets of small-signal models will be derived. The state variables for each model are slightly different Butthe control variables are the same. The decoupling networksrequired for both models to allow separate controller design.

Fig 6..Control scheme of the proposed three-port converter.

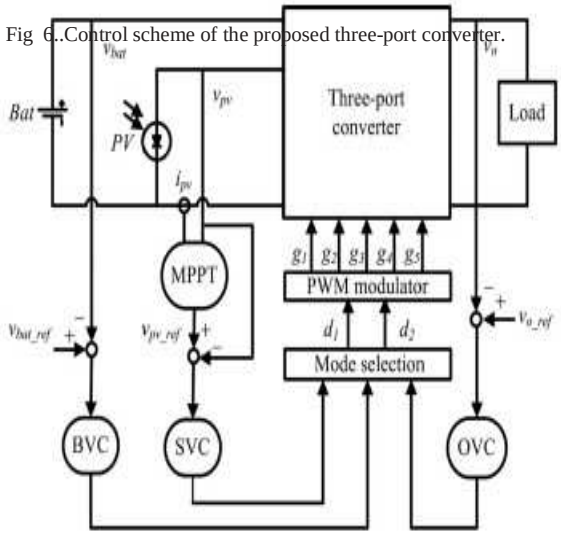

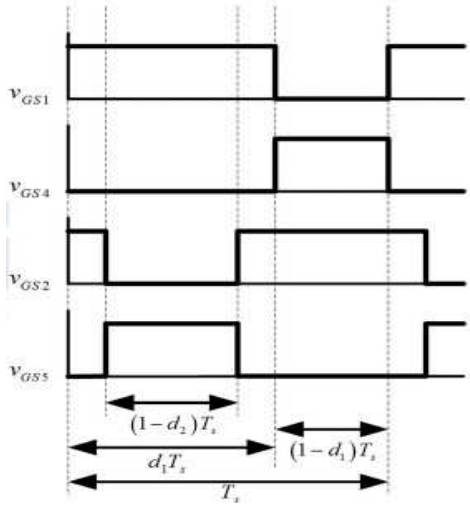

V.OPERATION OF PROPOSED SYSTEM

This paper has presented the topological principles, steady state analysis, and experimental results for a proposed converter. The proposed converter has been successfully implemented in an efficiently high step-up conversion without an extreme duty ratio and a number of turns ratios through the voltage multiplier module and voltage clamp feature. The interleaved PWM scheme reduces the currents that pass through each power switch and constrained the input current ripple by approximately 6%.

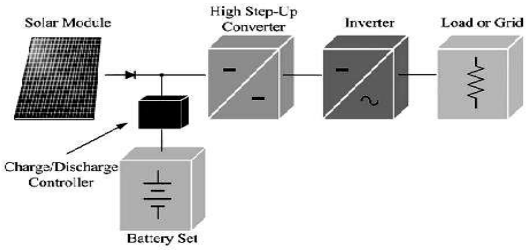

Fig 7. Topological PV System

The experimental results indicate that leakage energy is recycled through capacitors to the output terminal. Meanwhile, the voltage stresses over the power switches are restricted and are much lower than the output voltage (380 V). These switches, conducted to low voltage rated and low on-state resistance MOSFET, can be selected. Furthermore, the full load efficiency is 96.1% atpo=1000 W, and the highest efficiency is 96.8% at Po =400 W. Thus, the proposed converter is suitable for PV systems or other renewable energy applications that need high step-up high-power energy conversion

Fig. 9. Simulation Diagram

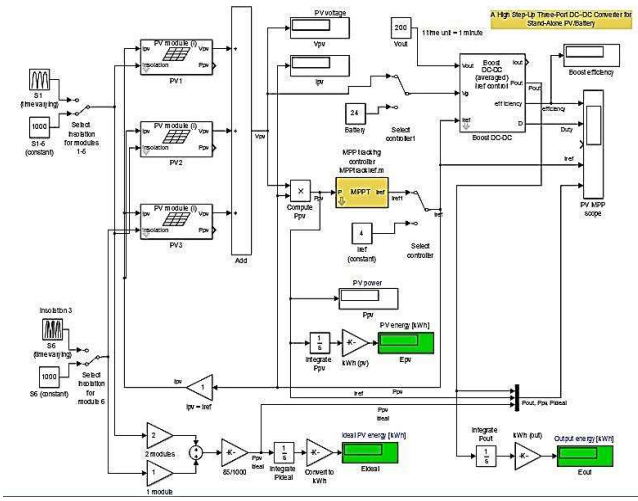

Fig 8. Simulation Output Wave Form

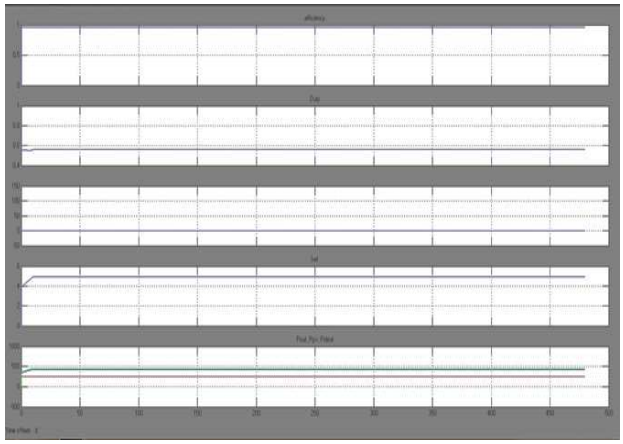

VI.CONCLUSION

A High step-up three-port DC–DC converter for stand-alone power systems is proposed to integrate solar and battery power. In the proposed topology, two coupled inductors are employed as voltage gain extension cells for high voltage output applications. Two sets of buck–boost type active-clamp circuits are used to recycle the energy stored in the leakage inductors and improve the efficiency. The proposed switching strategy only needs to control two duty ratios in different operation modes. The experimental results validate the functionality of the proposed converter under different solar irradiation level and load demand. The charging/discharging transitions of the battery could be achieved without changing the operation mode; therefore, the MPPT operation will not be interrupted. In light-load condition, once the charging voltage is higher than the present level, the operation mode will be changed rapidly to protect the battery from overcharging. The highest converter efficiency is measured as 90.1% at 110W. The control method of the battery port could be modified for the grid-connected applications.

REFERENCES

R. J. Wai, Ch. Y. Lin, J. J. Liaw, and Y. R. Chang, "Newly designed ZVS Multi-input converter," IEEE Trans. Ind. Electron., Feb. 2011.

F. Nejabatkhah, S. Danyali, S. H. Hosseini, M. Sabahi, and S. M. Niapour, "Modeling and control of a new three-input DC-DC boost converter for hybrid PV/FC/battery power system," IEEE Trans. Power Electron., Mar. 2008.

J. Jung and A. Kwasinski, "A multiple-input SEPIC with a bi-directional Input for modular distributed generation and energy storage integration," in Proc. IEEE Appl. Power Electron. Conf., 2011

S. H. Choung and A. Kwasinski, "Multiple-input DC-DC converter topologies comparison," in Proc. 34th Annu. Conf. IEEE Ind. Electron., 2008

A.Huang, "FREEDM system—a vision for the future grid," in Proc. IEEE Power Energy Soc. Gen. Meet., 2010

W. Li and X. He, "Review of nonisolated high-step-up DC/DC converters in photovoltaic grid-connected applications," IEEE Trans. Ind. Electron., Apr. 2011.

T.-F. Wu, Y.-S.Lai, J.-C.Hung and Y.-M. Chen, "Boost converter with Coupled inductors and buck–boost type of active clamp," IEEE Trans. Ind. Electron., Jan. 2008.

L. Nousiainen, J. Puukko, A. M¨aki, T. Messo, J. Huusari, J. Jokipii, J. Viinam¨aki, D. T. Lobera, S. Valkealahti, and T. Suntio, "Photovoltaic generator as an input source for power electronic converters?," IEEE Trans. Power Electron., Jun.